Am J Cancer Res 2023;13(2):638-653
www.ajcr.us /ISSN:2156-6976/ajcr0142145

Original Article

FOXA2 and STAT5A regulate oncogenic activity of KIF5B-RET fusion

Mi-Ran Lee[1,4], Jung-Young Shin[1], Min-Young Kim[1], Jeong-Oh Kim[1], Chan Kwon Jung[3], Jinhyoung Kang[2,4]

[1]Laboratory of Medical Oncology, Cancer Research Institute, College of Medicine, The Catholic University of Korea, Seoul, Republic of Korea; [2]Department of Medical Oncology, Seoul St. Mary's Hospital, The Catholic University of Korea, Seoul, Republic of Korea; [3]Department of Hospital Pathology, College of Medicine, The Catholic University of Korea, Seoul, Republic of Korea; [4]Department of Biomedicine & Health Sciences, The Catholic University of Korea, Seoul, Republic of Korea

Received February 2, 2022; Accepted January 19, 2023; Epub February 15, 2023; Published February 28, 2023

Abstract: *KIF5B-RET* gene rearrangement occurs in ~1% of lung adenocarcinomas. Recently, targeted agents that inhibit RET phosphorylation have been evaluated in several clinical studies; however, little is known about the role of this gene fusion in driving lung cancer. Immunohistochemistry was used to evaluate the expression of the FOXA2 protein in tumor tissues of patients with lung adenocarcinoma. KIF5B-RET fusion cells proliferated in a cohesive form and grew tightly packed with variable-sized colonies. The expression of RET and its downstream signaling molecules, including p-BRAF, p-ERK, and p-AKT, increased. In KIF5B-RET fusion cells, the intracellular expression of p-ERK was higher in the cytoplasm than in the nucleus. Two transcription factors, STAT5A and FOXA2, exhibiting significantly different expressions at the mRNA level, were finally selected. p-STAT5A was highly expressed in the nucleus and cytoplasm, whereas the expression of the FOXA2 protein was lower; however, it was much higher in the nucleus than in the cytoplasm. Compared with the expression of FOXA2 in the RET rearrangement-wild NSCLC (45.0%), high expression (3+) were observed in most RET rearrangement NSCLCs (94.4%). Meanwhile, KIF5B-RET fusion cells began to increase belatedly from day 7 and only doubled on day 9 in 2D cell culture. However, tumors in mice injected with KIF5B-RET fusion cells began to rapidly increase from day 26. In cell cycle analyses, the KIF5B-RET fusion cells in G0/G1 were increased on day 4 (50.3 ± 2.6%) compared with the empty cells (39.3 ± 5.2%; $P = 0.096$). Cyclin D1 and E2 expressions were reduced, whereas CDK2 expression slightly increased. pRb and p21 expression was diminished compared with the empty cells, TGF-β1 mRNA was highly expressed, and the proteins were accumulated mostly in the nucleus. Twist mRNA and protein expression was increased, whereas Snail mRNA and protein expression was decreased. Particularly, in KIF5B-RET fusion cells treated with FOXA2 siRNA, the expression of TGF-β 1 mRNA was remarkably reduced but Twist1 and Snail mRNA were increased. Our data suggest that cell proliferation and invasiveness in KIF5B-RET fusion cells are regulated by the upregulation of STAT5A and FOXA2 through the continuous activation of multiple RET downstream signal cascades, including the ERK and AKT signaling pathways. We found that TGF-β1 mRNA, where significant increments were observed in KIF5B-RET fusion cells, is regulated at the transcriptional level by FOXA2.

Keywords: KIF5B-RET gene fusion, p-ERK, FOXA2, STAT5A, TGF-β1

Introduction

RET is a transmembrane receptor tyrosine kinase with a unique extracellular domain included [1]. It is a receptor tyrosine kinase involved in cell proliferation, neuronal navigation, cell migration, and cell differentiation [2]. *RET* acts via overexpression, mutation, and fusion, and it is considered a novel therapeutic target in various cancers [3, 4].

RET fusions account for 1-2% of patients with lung cancer, and at least 15 fusions have been reported [5, 6]. Chromosomal fusion between the *RET* gene and other domains, such as *KIF5B* and *CCDC6* in NSCLC, causes the overexpression of the RET protein; 70-80% of KIF5B-RETs and 20-30% of CCDC6-RETs have been identified [7]. RET fusion inhibitors have been used in the past as multi-kinase inhibitors, and have generally yielded poor results. Recently, studies

on selective RET inhibitors (selpercatinib, pralsetinib) have revealed that they induce a significant and sustained tumor response in patients who have received a lot of pre-treatment; however, the mechanism of resistance to them is not clear [8]. The median survival of patients with *KIF5B-RET* was shorter than that of those with *CCDC6-RET* [7].

KIF5B-RET is a novel gene fusion of the kinesin family member 5B gene (*KIF5B*), which is combined with the rearranged during transfection gene (*RET*) resulting from a chromosome 10 inversion (p11; q11). It was first identified in a nonsmoking Korean young male as an adenocarcinoma via whole-genome and transcriptome sequencing [9]. *KIF5B-RET*, which occurs in a low percentage of lung cancers, is more frequent in non-smokers and in patients with adenocarcinoma. It occurs exclusively with other mutations, such as *EGFR*, *K-RAS*, *B-RAF*, *ErbB2*, or *EML4-ALK* fusions [3, 10, 11].

There are seven components identified in the transcription factor family of Signal transducer and activator of transcriptions (*STAT*) and *STAT3/5*, which are oncogenic transcription factors of the JAK-STAT pathway [12, 13]. *STAT5A* is a transcription factor activated by various cancer-related cytokines and growth factors. It also plays a key role in maintaining tumor differentiation and inhibiting disease progression in cancer [13, 14]. However, the role of *STAT5A* in lung tumorigenesis is unclear.

Forkhead box transcription factor (*FOXA2*) is a transcription factor that plays a "pioneer" role in regulating transcription. It regulates expression during lung morphogenesis and differentiation and is highly expressed in bronchial and alveolar type II cells [15-17]. *FOXA2* expression is found to be decreased in many lung cancer cell lines compared to normal lung cells [18]. In several cancers, *FOXA2* not only has ambivalent functions progression or suppression [19-21] but also plays an important role in tumorigenesis and metastasis through regulation together with *FOXA1* [22, 23] and *FOXA3* [24].

KIF5B-RET-positive lung cancer patients show poor drug response and poor prognosis compared to patients with other rearrangement. It is unclear how KIF5B-RET activates specific downstream signaling pathways during cancer initiation and progression. In this study, we examined changes in cell proliferation and migration and the expression of RET downstream signaling molecules by the *KIF5B-RET* gene fusion.

Materials and methods

Cells and tumor tissues

HEK293T (ATCC, Cat#: CRL-3216, USA) cells were maintained in DMEM (Welgene, Cat#: LM001-05, Korea) supplemented with 10% fetal bovine serum (FBS, RM Bio, Cat#: FBS-BBT, MT, USA), 100 U/mL penicillin, and 100 μg/mL streptomycin (Gibco, Cat#: 15140122, CA, USA). The presence of the *KIF5B-RET* gene fusion was determined in tumor tissues collected from NSCLC patients at Seoul St. Mary's Hospital and the Korea Lung Tissue Bank using RT-PCR and Nanostring analyses.

The pLOC viral expression vector containing the *KIF5B-RET* gene fusion (K16:R12) plus green fluorescent protein (GFP) was obtained from Open Biosystems (Huntsville, AL). The virus was packaged using the Viral Power Packaging system (Invitrogen, CA, USA) per the manufacturer's instructions. The virus was collected via centrifugation at 3,000 rpm for 15 min. The nucleotide sequence and direction of both plasmids were verified via DNA sequencing. HEK293T cells, in which all lentiviral vectors were packaged, were co-incubated with viruses containing pLOC alone or the pLOC/*KIF5B-RET* gene fusion (K16:R12)/GFP for 48 h before adding blasticidin (2.5 μg/ml, Invitrogen, Cat#: R21001, CA, USA). The efficiency of transduction of GFP-expressing constructs was checked via immunofluorescence microscopy, and the mRNA and protein expressions of the *KIF5B-RET* gene fusion and the *RET* gene were analyzed by RT-PCR and western blot, respectively.

Cell proliferation and clonogenic assays

Cell proliferation was measured using the Cell Counting Kit-8 assay (Dojindo, Cat#: CK04, Japan). The cells were suspended in the DMEM medium supplemented with 10% heat-inactivated FBS and subsequently seeded into a 96-well plate and incubated for nine days. Next, a 10-μL aliquot of the CCK-8 solution was added to each well and incubated at 37°C for 4 h. The optical density (OD) value of absorbance at 450 nm was measured using an ELISA reader (PowerWave XS, BIO-TEK, VT, USA). The

results were plotted as the mean ± SD of three independent experiments per sample. Cells were plated in 9-cm dishes with 1,000 cells/well at 24 h following irradiation and maintained for 10 days to allow colony formation. Once visible colonies (at least 50 cells) emerged, they were fixed with 95% methanol, stained with 0.5% crystal violet, and counted via microscopy.

Reverse transcription-polymerase chain reaction (RT-PCR)

Total RNA was extracted using TRIzol Reagent (ambition, Cat#: 15596026, CA, USA) per the manufacturer's protocol. The concentration and purity of RNA were determined by A260 and the A260/A280 ratio, respectively. The integrity of the RNA was assessed on 1% agarose/formaldehyde gels. cDNA was obtained from 1 μg of total RNA using the maxime RT PreMix kit (intronbio, Cat#: 25081, Korea) in a final volume of 20 μl. The cDNA (1 μl for each sample) was amplified by PCR using the primers listed in Table S1. Thermal cycling conditions: 95°C for 2 min, 35 cycles of 95°C for 30 sec, 52°C-60°C, depending on the Tm of each individual set of primers, for 1 min and at 72°C for 30 sec. GAPDH was amplified as an internal control. The RT-PCR products were separated via 2% agarose gel electrophoresis, stained with ethidium bromide, and then photographed under a UV illuminator.

Western blot analysis

Protein was extracted from empty vector-transfected cells and KIF5B-RET gene fusion-transfected cells and prepared in a sample loading buffer [0.125 M Tris/HCl (pH 6.8), 4% (w/v) SDS, 20% (v/v) glycerol and 10% (v/v) 2-mercaptoethanol]. Approximately 40 μg of protein was resolved by SDS/PAGE (10% gels) and transferred to PVDF membranes (0.45 um pore, Merck Millipore, Cat#: IPVH00010, MA, USA). The membranes were blocked for 1 h at room temperature with 5% (w/v) non-fat dried skim milk powder prepared in TBST (Tris-buffered saline (iNtRON Biotechnology, Cat#: IBS-BT005-1, Korea) with 0.1% Tween 20 (Biosesang, Cat#: T1072, Korea)). The membranes were probed with antibodies against RET downstream signaling molecules; RET (Cat#: 3223), p-AKT (Cat#: 4060), p-ERK (Cat#: 9101; Cell Signaling technology, MA, USA), p-BRAF (Abcam, Cat#: ab68215, UK), cell cycle regulators; Cyclin A2 (Cell signaling technology, Cat#: 4656, MA, USA), Cyclin D1 (Santa Cruz Biotechnology, Cat#: sc-20044, CA, USA), Cyclin E2 (Cell signaling technology, Cat#: 4132, MA, USA), CDK4 (Cell signaling technology, Cat#: 12790, MA, USA), and CDK2 (BD bioscience, Cat#: 51-9001931, NJ, USA), apoptosis-related molecules; pRb (Cat#: 9308), p-p53 (Cat#: 9284), p21 (Cat#: 2947; Cell Signaling technology, MA, USA), and FOXA2 (Santa Cruz Biotechnology, Cat#: sc-101060, CA, USA), phospho-stat5A (Santa Cruz Biotechnology, Cat#: sc-101806, CA, USA) 1:1000 dilution; overnight at 4°C. After washing, the membranes were incubated for 30 min at room temperature with the appropriate HRP (horseradish peroxidase)-conjugated secondary antibodies and subsequently developed with the ECL® (enhanced chemiluminescence) western blotting system (PXi4; Syngene, Cambridge, UK). β-Actin (Cat#: G043) and GAPDH (Cat#: G041) were used as the internal loading controls and detected with specific antibodies (1:1000 dilution; abm, WA, USA).

Flow cytometric analysis

Cell cycle distribution was determined via flow cytometry as previously described. Empty vector- or *KIF5B-RET* gene fusion-transfected cells were seeded into 6-well plates under standard culture conditions. After incubation for 1 or 4 days, the culture medium was aspirated, and then the cells were quickly washed twice with ice-cold PBS and trypsinized. Then, the cell pellet was harvested. For cell cycle analyses, cells were fixed in ice-cold ethanol (70%) and then stored at 4°C overnight. Before the analysis, the cells were washed twice with PBS, suspended in 0.5 mL of cold propidium iodide solution (PI) containing 10 μL of RNase A (25 μg/mL) and 10 μL of PI (50 μg/mL), and then incubated at 37°C for 30 min in the dark. Subsequently, the cell cycle distribution was determined by analyzing 10,000 conjugated cells using a FACScan cytometer with Cell Quest software (FACSCalibur; Becton-Dickinson, CA, USA). All experiments were performed in triplicate.

Migration and wound-healing assay

The cell migration assay was conducted using 24-well Transwell inserts (8-μm pore, Corning

Costar Corp., Cat#: 9328012, MA, USA). Cells were seeded in the upper chamber at 2 × 10^4 cells/ml in a medium containing 0.1 ml of 1% FBS. The medium, supplemented with 10% FBS, was placed in the bottom compartment in a volume of 0.8 ml, which is used as a chemoattractant. After incubation for 24 h at 37°C in an atmosphere containing 5% CO_2, the cells on the upper surface of the insert membrane were removed with cotton swabs, and the migrating cells were fixed and stained with 0.05% crystal violet. The migrated cells from each insert were counted using a microscope at 200 × magnification (LEICA, CAT#: DM IRB/DC300, Germany). For wound-healing assays, a scratch was made across the cell monolayer using a sterile tip. The ability of the cells to migrate was monitored at the zero-time point and at subsequent time points via light microscopy. At least three independent experiments were conducted.

Expression of transcription factor mRNA by PCR

RNA was isolated from empty vector-transfected cells and KIF5B-RET gene fusion-transfected cells. The RT2 Profiler PCR Array (SABiosciences, Qiagen, Cat#: 330231, France) was used to examine the expression patterns of 84 genes involved in endothelial cell biology. The manufacturer's instructions were strictly followed. The components were mixed in a 5-ml tube or a multi-channel reservoir: 550 µl of 2X SuperArray PCR master mix, 102 µl of a diluted first-strand cDNA synthesis reaction, and 448 µl of ddH_2O. The cocktail was then added to the PCR array. Real-time PCR was performed under the following thermal cycling conditions: 95°C for 10 min; 40 cycles of 95°C for 15 sec, and 60°C for 1 min. Gene expression levels were analyzed using the web-based "RT2 Profiler PCR Array data analysis software supplied by Qiagen (-version 3.5)". *P*-values were calculated based on Student's t-test of the replicate $2^{\Delta\Delta Ct}$ values for each gene in the empty cells and the KIF5B-RET gene fusion-transfected cells. We set the threshold for the *P*-values at 0.05 for the volcano plot presentation.

RNA interference

One day after seeding, the cells were transfected with double-stranded siRNA (25 µmol/L) against FOXA2 (Santa Cruz Biotechnology, Inc., USA) using Lipofectamine 2000 (Invitrogen, Cat#: 11668-027, CA, USA). Non-specific siRNA-transfected cells served as a control. The siRNA-transfected cells were cultured in the presence or absence of FOXA2. Total cell lysates were prepared to evaluate the mRNA expression of FOXA2 and epithelial-to-mesenchymal transition (EMT) markers by RT-PCR. FOXA2 siRNA sequences were as follows: FOXA2 siRNA 1: GAACAUGUCGUCGUACGUG; FOXA2 siRNA 2: GCAGAUACCUCCUACUACC.

In vivo studies

BLAB/c nude mice (Female, 4-6-week-old) were obtained from Orient-Bio Korea. Empty vector and KIF5B-RET gene fusion cells (1 × 10^6/100 µl) were subcutaneously injected into the mice. The tumor volume was calculated using the formula: V (mm^3) = length × $width^2$ × 1/2. All animal procedures were conducted per the Laboratory Animals Welfare Act, the Guide for the Care and Use of Laboratory Animals, and the Guidelines and Policies for Rodent experiments provided by IACUC (Institutional Animal Care and Use Committee) in the School of Medicine, The Catholic University of Korea (Approval number: CUMS-2020-0152-02). IACUC and the Department of Laboratory Animals in the Catholic University of Korea, Songeui Campus accredited the Korea Excellence Animal laboratory facility from the Korea Food and Drug Administration in 2017 and acquired AAALAC International full accreditation in 2018. The mouse-rearing environment was maintained at a temperature of 20°C-26°C and 50% ± 10% humidity with a 12-hour light-dark cycle. Mice were fed with a gamma ray-sterilized diet (TD 2018S, Harlan Laboratories Inc., America) and provided autoclaved reverse osmosis (R/O) water and Aspen bedding (PG-3, LAS bedding, Germany).

Histological and immunohistochemical analysis

Hematoxylin and Eosin (H&E) stain and immunohistochemistry (IHC) were performed. Briefly, 4-µm paraffin-embedded tissue sections were deparaffinized with xylene. Endogenous peroxidase activity was blocked by immersing the sections in methanol with 3% hydrogen peroxide for 10 min, after which they were washed with water and PBS. Antigen retrieval was performed by boiling the sections in citrate buffer

(ScyTek laboratories, Cat#: CBB500, UT, USA). The tissue sections were incubated with FOXA2 (Cat#: 22474-1-AP) and STAT5A (Cat#: 13179-1-AP) antibody (Protein Tech Group, IL, USA) at 4°C overnight using a predetermined optimal dilution (1:100). The slides were washed with PBS and then incubated with the biotinylated secondary antibody (Polink2 plus HRP Rabbit DAB kit; GBI Labs, Cat#: D41-125, WA, USA) for 10 min at room temperature. After washing with water and PBS, the peroxidase activity was developed with 3, 3'-diaminobenzidine (DAB). The sections were counterstained with hematoxylin and imaged. Finally, the expression levels of FOXA2 and STAT5A were scored on the basis of the staining intensity of the tumor cells and the relative proportion of positively-stained cells among the total tumor cells. The tumor cell staining intensity was graded as follows: 0: absent; 1: weak (light brown); 2: moderate (brown); and 3: strong (dark brown). Multiplying the percentage score by the intensity score yielded a semiquantitative score.

Statistical analysis

Statistical analyses were performed using PASW Statistics version 18.0 (SPSS Inc., Chicago, IL, USA). All quantitative data were expressed as the mean ± standard error of the mean. Differences between groups were analyzed using the one-way analysis of variance followed by Scheffe's post-test. The statistical significance of differences was determined using Student's t-test. *P*-values of < 0.05 were considered statistically significant ($^{*}P < 0.05$; $^{**}P < 0.01$).

Results

The change of cell morphology and activation of RET downstream signaling in KIF5B-RET fusion cells

We confirmed the introgression of the KIF5B-RET gene fusion through GFP expression and mRNA transcript and protein expression in HEK293T-transformed cells (**Figure 1A-C**). Morphologically, the KIF5B-RET fusion cells proliferated in a cohesive form and grew tightly packed with variable-sized colonies (**Figure 1D**).

When we checked the RET protein and its downstream signaling molecules in KIF5B-RET fusion cells, p-BRAF, p-ERK, and p-AKT were increased (**Figure 1E**). The p-ERK and p-AKT expression gradually increased in the empty cells over time; whereas, in KIF5B-RET fusion cells, p-ERK expression increased over time while p-AKT expression remained unchanged. Interestingly, in KIF5B-RET fusion cells, the intracellular expression of p-ERK was much higher in the cytoplasm than in the nucleus. Compared with empty cells, p-ERK expression was lower on day 3; however, it became relatively high on day 7. Meanwhile, p-AKT expression in KIF5B-RET fusion cells was slightly higher in the cytoplasm than in the nucleus; however, the expression pattern in the cytoplasm was similar to that in the nucleus. p-AKT expression was higher in KIF5B-RET fusion cells than in the empty cells on day 3 but no difference in expression was observed on day 7 (Figure S1A).

Selection of putative transcription factors in KIF5B-RET fusion cells

Using a cDNA microarray and transcription factor PCR array, we evaluated the expression of genes and transcription factors to identify downstream signaling molecules influenced by the KIF5B-RET gene fusion. The cDNA microarray analysis revealed 1,172 genes that were significantly differentially expressed between KIF5B-RET fusion cells and empty cells. Of these, 535 genes showing identical expression levels between the two subclones of KIF5B-RET fusion cells were selected. Compared with the expression profile in empty cells transfected with the empty vector, there were 39 genes in which the expression level was elevated more than two-fold. Additionally, expression increased by at least three-fold was observed in only 3 genes: 5.3-fold for RPL22L1, 4.5-fold for MGST1, and 3.0-fold for SNTB1. There were 28 genes in which the expression level was decreased by more than two-fold: -4-fold for ITM2A, MAP7D2, and HES5, -3.7-fold for MAOA and LOC644695, -3.4-fold for BEX1, and -3.0-fold for BASP1 (Figure S2A). To investigate changes in the expression of transcription factors by the KIF5B-RET gene fusion, we screened 90 transcription factors in KIF5B-RET fusion cells using a PCR array. Three transcription factors (AR, ID1, and MYOD1) in the KIF5B-RET fusion cells exhibited a 1.5-fold lower expression than the empty cells with the greatest difference observed for AR (16.1-fold). Meanwhile,

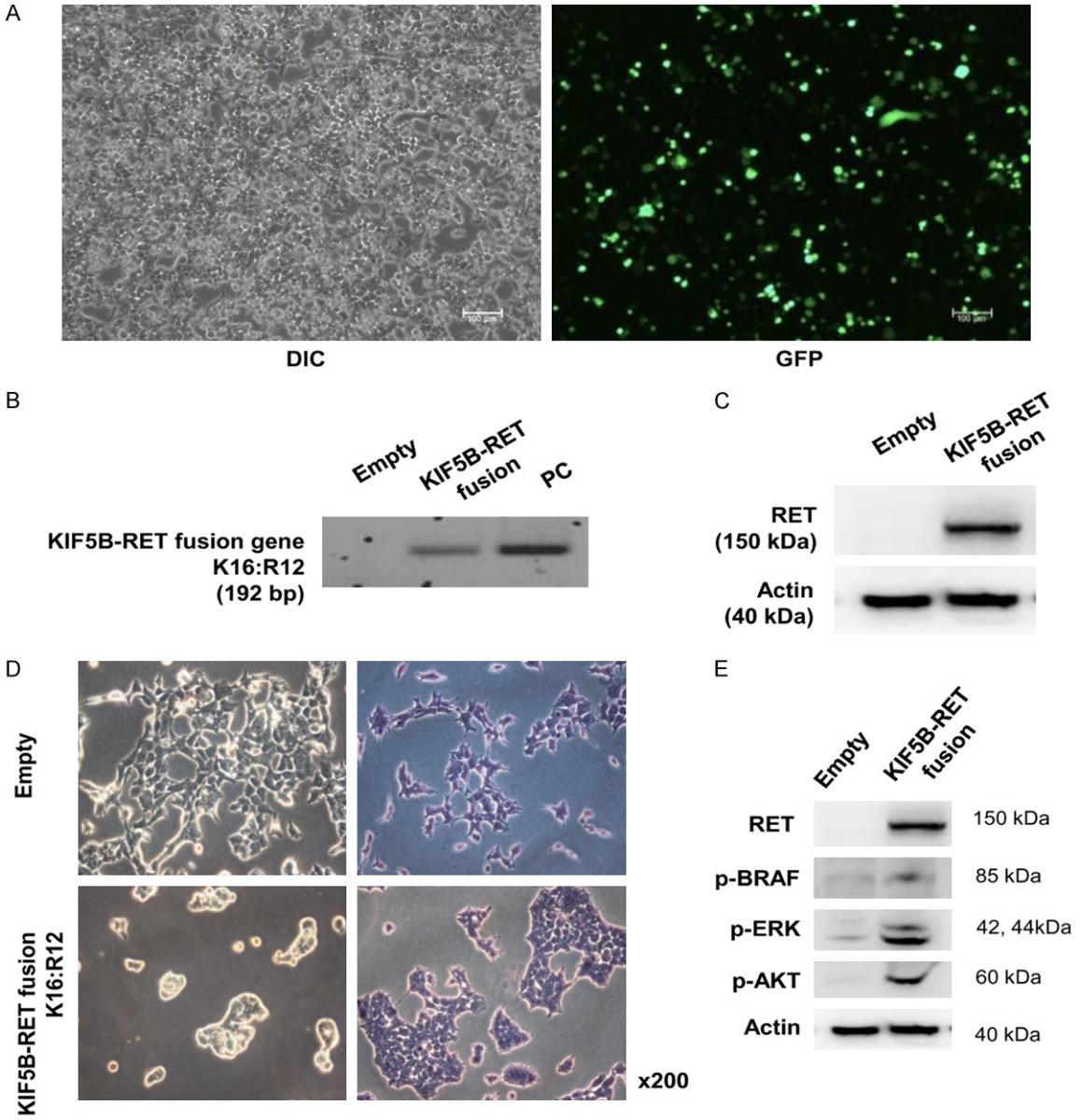

Figure 1. Morphological differences and RET downstream signaling pathways in KIF5B-RET fusion cells. A. Establishment of the KIF5B-RET gene fusion using confirmed DIC and GFP. B. The KIF5B-RET gene fusion (KIF5B exon 16:RET exon 12) and total RET expression were analyzed using RT-PCR and western blot, respectively. C. Levels of RET expression in empty vector and KIF5B-RET fusion-transformed cells. D. Cell morphological differences between the empty vector and KIF5B-RET fusion-transformed cells were observed for the KIF5B-RET gene fusion. (Right: H&E staining, left: light microscopy). E. RET downstream signaling molecules were identified via western blot analyses.

the mRNA expression of transcription factors, MYF5 (1.6-fold), STAT5A (1.6-fold), and FOXA2, were significantly increased with the highest expression in FOXA2 (4.6-fold; Figure S2B). We compared the genes displaying significant differences in expression in the cDNA microarray with target genes controlled by the six transcription factors identified by the PCR array. The genes that were commonly differentially expressed between the cDNA microarray and transcription factor PCR array were CCND2, CCNB1IP1, UBE3A, NFkB1B, and MDM2 (**Figure 2A**). We examined the expression of two transcription factors (FOXA2 and STAT5A) in the mRNA and protein levels. In KIF5B-RET fusion cells, FOXA2 and STAT5A were highly expressed at the mRNA and protein levels (**Figure 2B**). Additionally, we observed the expression of two

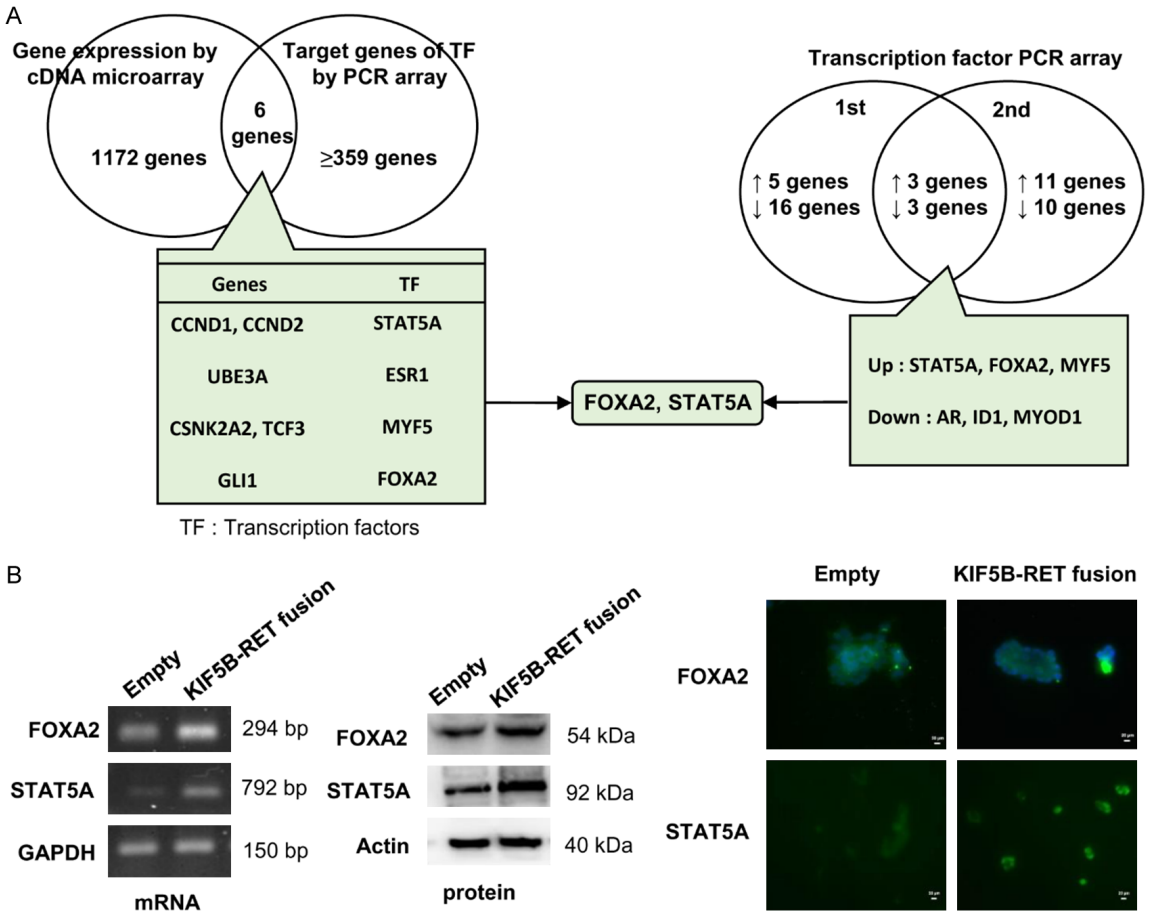

Figure 2. Selection of transcription factors upregulated in the KIF5B-RET gene fusion. A. Schematic diagram of selected transcription factors. B. Increased FOXA2 and STAT5A caused by the KIF5B-RET gene fusion were assessed via RT-PCR, western blot (left), and immunofluorescence staining (right).

transcription factors (FOXA2 and STAT5A) in the nuclei and cytoplasms over time. The expression of the FOXA2 protein was relatively lower in KIF5B-RET fusion cells compared with the empty cells and was higher in the nucleus than in the cytoplasm. In the empty cells, the expression of FOXA2 protein did not change in the nucleus but increased in the cytoplasm with time, whereas the expression of FOXA2 remained unchanged in the nuclei and cytoplasms of KIF5B-RET fusion cells. p-STAT5A was highly expressed in the nuclei and cytoplasms of KIF5B-RET fusion cells; however, no changes were observed over time (Figure S1B).

FOXA2 expression in NSCLC patients harboring the RET rearrangement

To determine the difference in FOXA2 expression depending on the existence of the RET rearrangement in the tumor tissue, IHC was performed with 38 tumor specimens from NSCLC patients who had already confirmed for the presence of RET rearrangement by RT-PCR and Nanostring technology in our previous study. We analyzed the expression of FOXA2 according to the staining intensity in IHC. When compared with the wild type cases (45.0%), high expression of FOXA2 was observed in most RET rearrangement cases (94.4%; **Table 1**; **Figure 3**). Using immunohistochemistry, we investigated the expression of FOXA2 and STAT5A in NSCLC patients with/without RET rearrangement. The expression of FOXA2 and STAT5A was strongly stained in the nucleus in NSCLC patients carrying the RET rearrangement (data not shown).

Cell proliferation and migration in KIF5B-RET fusion cells

To examine the influence of the *KIF5B-RET* gene fusion on cell growth, we measured the

Table 1. Immunohistochemistry of FOXA2 in 38 patients with lung adenocarcinoma between wild type and RET rearrangement

Staining intensity	Lung adenocarcinoma	
	Wild type (%) (N = 20)	RET rearrangement (%) (N = 18)
0	5 (25.0)	-
1+	3 (15.0)	1 (5.6)
2+	3 (15.0)	-
3+	9 (45.0)	17 (94.4)

The expression level of FOXA2 was graded on the basis of the staining intensity of tumor cells. Multiplying the percentage score by the intensity score yielded a semi-quantitative score.

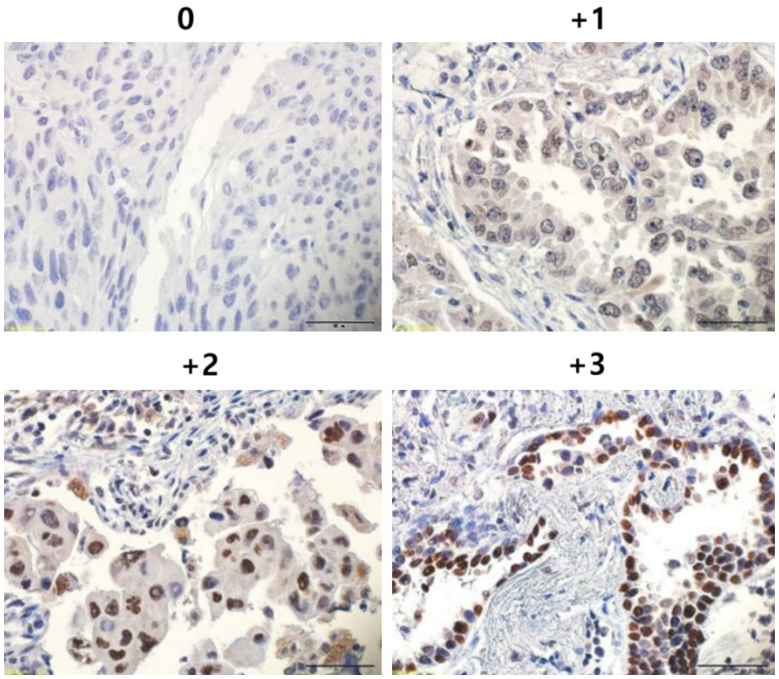

Figure 3. The expression of FOXA2 as assessed via IHC analysis. Staining intensity was scored as follows: 0: absent; 1: weak; 2: moderate; and 3: strong. Bar = 50 μm.

proliferation rate of KIF5B-RET fusion cells. The OD values of the empty cells gradually increased during the first five days of the incubation period and reached 2.5- and 7-fold exponential increments on days 7 and 9, respectively. In contrast, the OD value in the KIF5B-RET fusion cells began to increase belatedly from day 7, and it was not until day 9 that it doubled. Colony formation was also delayed, even with the long-term culture of 10-15 days (**Figure 4A**). In addition, we measured the diameter of the spheroids as a function of time to determine the proliferative activity of KIF5B-RET fusion cells in a three-dimensional cell culture system. On days 3 and 10, the mean diameters of the spheroids of KIF5B-RET fusion cells were 268.5 ± 5.5 μm and 333.8 ± 5.9 μm, respectively, whereas the empty cells had diameters of 225.8 ± 4.1 μm and 305.4 ± 7.4 μm, respectively. The empty cells increased by 19.6%, whereas KIF5B-RET fusion cells increased by 26.1% (data not shown). Unlike the cell proliferation rate observed in two-dimensional cell culture, the rate tended to increase in the spheroids of KIF5B-RET fusion cells. In an *in vivo* experiment, we assessed the changes in tumor volume using a xenograft model transplanted with KIF5B-RET fusion cells compared with that of the control mice. Tumors in mice injected with KIF5B-RET fusion cells began to increase from day 26 and significantly differed from that of the controls on day 33 (**Figure 4B**). Immunochemical staining revealed that RET and HIF1α were highly expressed in the tumor specimens collected from mice bearing KIF5B-RET fusion cells (**Figure 4C**).

We performed a wound-healing assay to evaluate the influence of the KIF5B-RET gene fusion on cell migration. The empty cells migrated to ~80% of the cell-free area after 24 h; however, KIF5B-RET fusion cells encompassed less than 30% of the scratched area (Figure S3). The results of cell migration through a Boyden chamber yielded similar results to that of the wound-healing assay (data not shown).

Change in cell cycle distribution and RET downstream signaling of KIF5B-RET gene fusion cells

To determine the effect of the KIF5B-RET gene fusion on the cell cycle, we analyzed the changes in cell cycle distribution for each phase between days 1 and 4. On day 1, the cell popu-

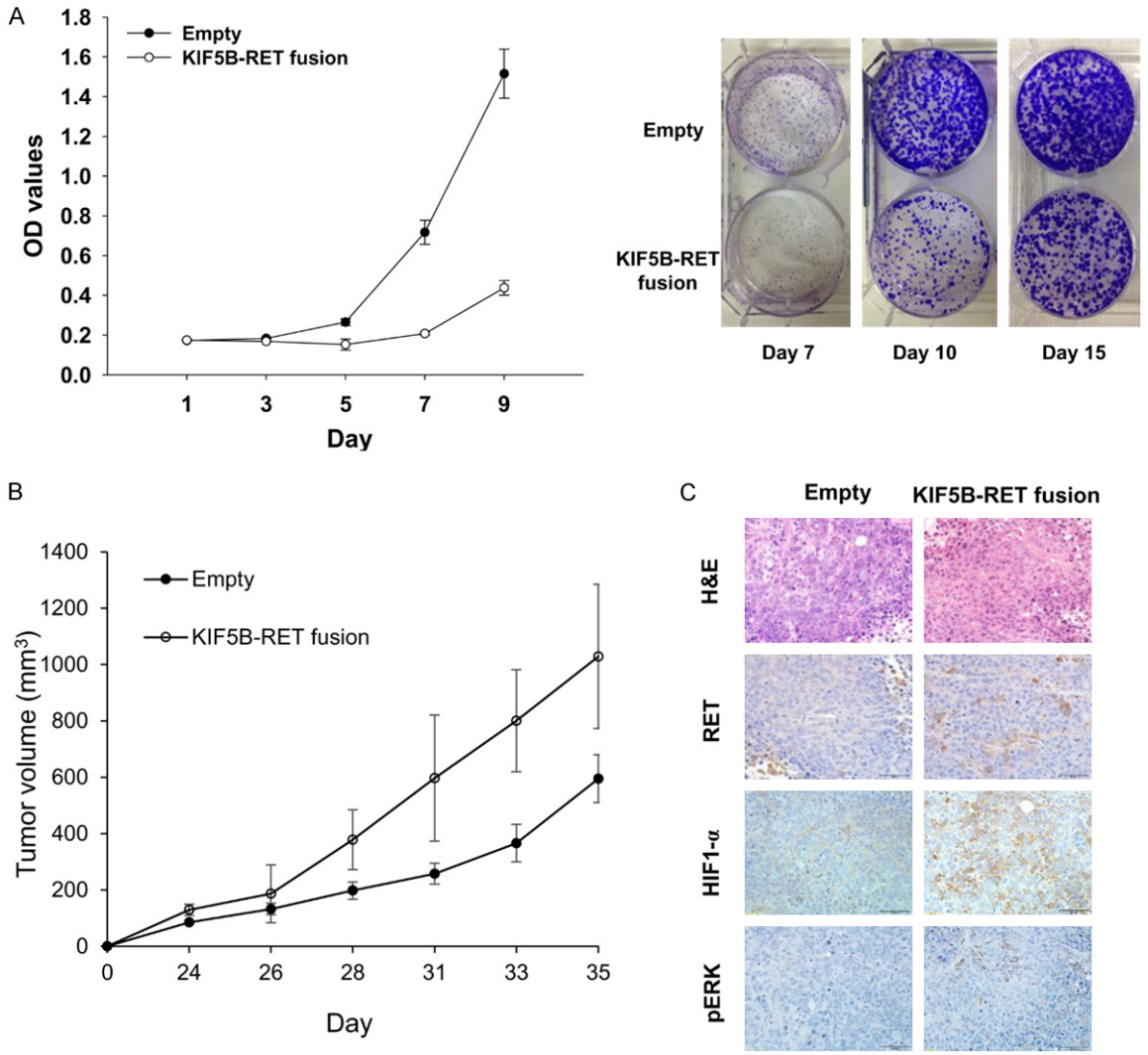

Figure 4. Difference in proliferation with the KIF5B-RET gene fusion. A. Expression of the KIF5B-RET fusion decreased the cell proliferation rate *in vitro*. Empty and KIF5B-RET fusion cell lines were seeded into 96-well plates at 1,000 cells/well. (Right: colony assay, left: cell proliferation CCK8 assay). B. The changes in tumor volume using a xenograft model injected with KIF5B-RET-transformed cells compared with that of the Empty mice. C. H&E staining (top) and IHC staining (bottom) were performed for RET, HIF1α, and p-ERK in empty and KIF5B-RET-transformed mice groups. The data are presented as the mean ± SE.

lation in the G0/G1 phase was similar between the KIF5B-RET fusion cells and empty cells (42.9 ± 3.6% vs. 45.6 ± 3.2%, respectively). However, on day 4, the cell population in G0/G1 was increased (50.3 ± 2.6%) in KIF5B-RET fusion cells compared with the empty cells (39.3 ± 5.2%; P = 0.096; **Figure 5A**). With respect to cell cycle regulators in KIF5B-RET fusion cells, cyclin D1 and E2 expressions were markedly reduced, whereas CDK2 expression was slightly increased. Phosphorylated Rb and p21 expressions were diminished compared with the empty cells; however, no change in phosphorylated p53 expression was observed (**Figure 5B**). We evaluated the changes in the protein expression of these cell cycle regulators over time. Compared with the empty cells in which expression gradually increased on days 7 and 10, cyclin D1 expression in KIF5B-RET fusion cells increased on day 7 and decreased thereafter. Cyclin E2 remained unchanged at a low expression level from day 3 (Figure S4A).

The expression of EMT markers in KIF5B-RET fusion cells knocked down by FOXA2 siRNA

We investigated the expression of EMT-related molecules in KIF5B-RET fusion cells. TGF-β

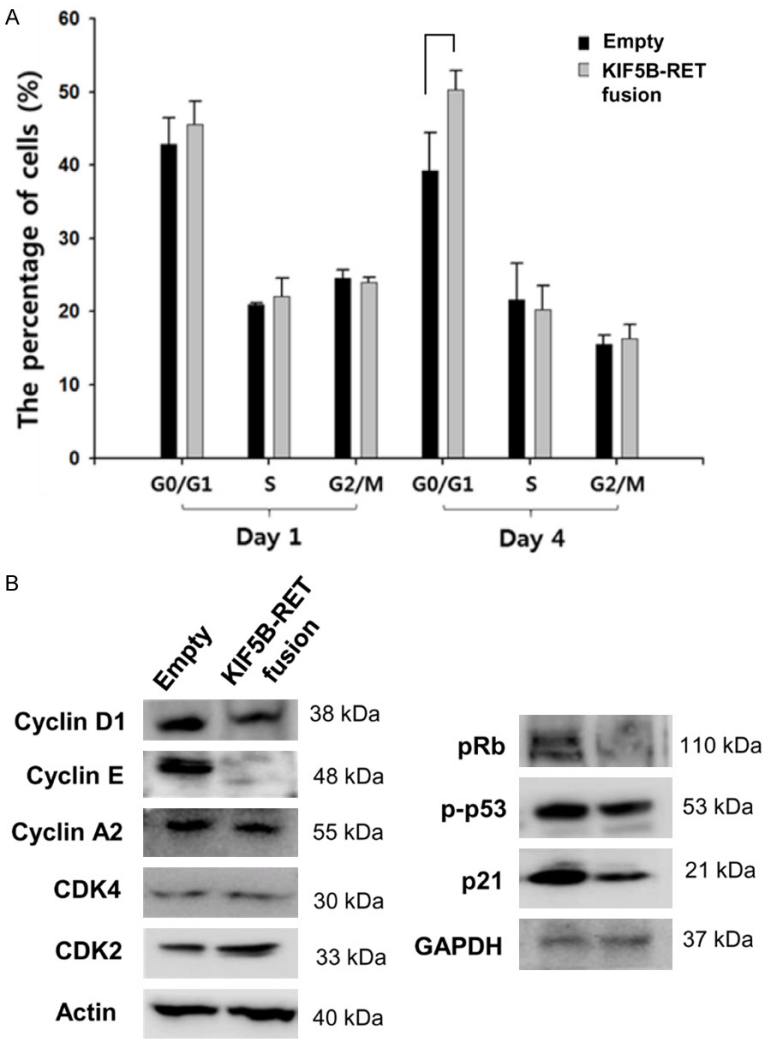

Figure 5. Identification of cell cycle expression in KIF5B-RET fusion cells. A. Cell cycle distribution was measured via flow cytometry for different time points (Day 1 or Day 4). Statistical analyses of the cell cycle phase distribution in the empty cells and KIF5B-RET fusion cells. B. The level of cell cycle-related molecules, including CDK2, CDK4, and cyclins D1 E2, A2, and pRb, p-p53, p21. The data are presented as the mean ± SE. *denotes $P < 0.05$ and **denotes $P < 0.01$.

mRNA was highly expressed, and the protein expression did not differ from that of the empty cells. However, it was accumulated in KIF5B-RET fusion cells rather than empty cells in the nucleus. No significant differences were evident between E-cadherin and Vimentin protein expression. In KIF5B-RET fusion cells, Twist mRNA and protein expression were increased, whereas Snail mRNA and protein expression were decreased. The mRNA expression of N-cadherin was increased but the protein expression was decreased (**Figure 6A**). The expression of FOXA2 mRNA, a transcription factor identified in a prior experiment, reached its lowest level on day 7; however, it increased again after day 10, which was a similar pattern to that of Twist1. In contrast, the expression of N-cadherin mRNA was highest on day 7 and the expression of Snail mRNA remained unchanged over time, unlike that in the empty cells (Figure S4B).

We evaluated the expression of EMT markers following the knockdown FOXA2 mRNA expression via the treatment of KIF5B-RET fusion cells with FOXA2 siRNA. After treatment, the expression of FOXA2 mRNA in the empty cells and KIF5B-RET fusion cells was reduced by 1.8- and 2.8-fold ($P = 0.034$ vs. $P = 0.007$, respectively). In particular, in KIF5B-RET fusion cells treated with FOXA2 siRNA, the expression of Twist1 mRNA was increased 2.3-fold ($P = 0.018$) by the reduced FOXA2 expression (vs. 1.5-fold increase in empty cells, $P = 0.020$), and a 1.4-fold ($P = 0.018$) increase in Snail mRNA (vs. 2.7-fold increase in empty cells, $P = 0.031$; **Figure 6B**). We used a Boyden chamber to evaluate cell mobility resulting from reduced FOXA2 mRNA expression; however, no significant differences were observed (data not shown).

Discussion

RET rearrangement is a driver genetic alteration found in a subset of lung adenocarcinoma [3, 10, 11, 25]. It is more commonly detected in never smokers and younger patients [26]. However, not only the role of RET rearrangement but also its downstream signaling pathways in cancer development and progression have not been well understood. In *in vitro* and

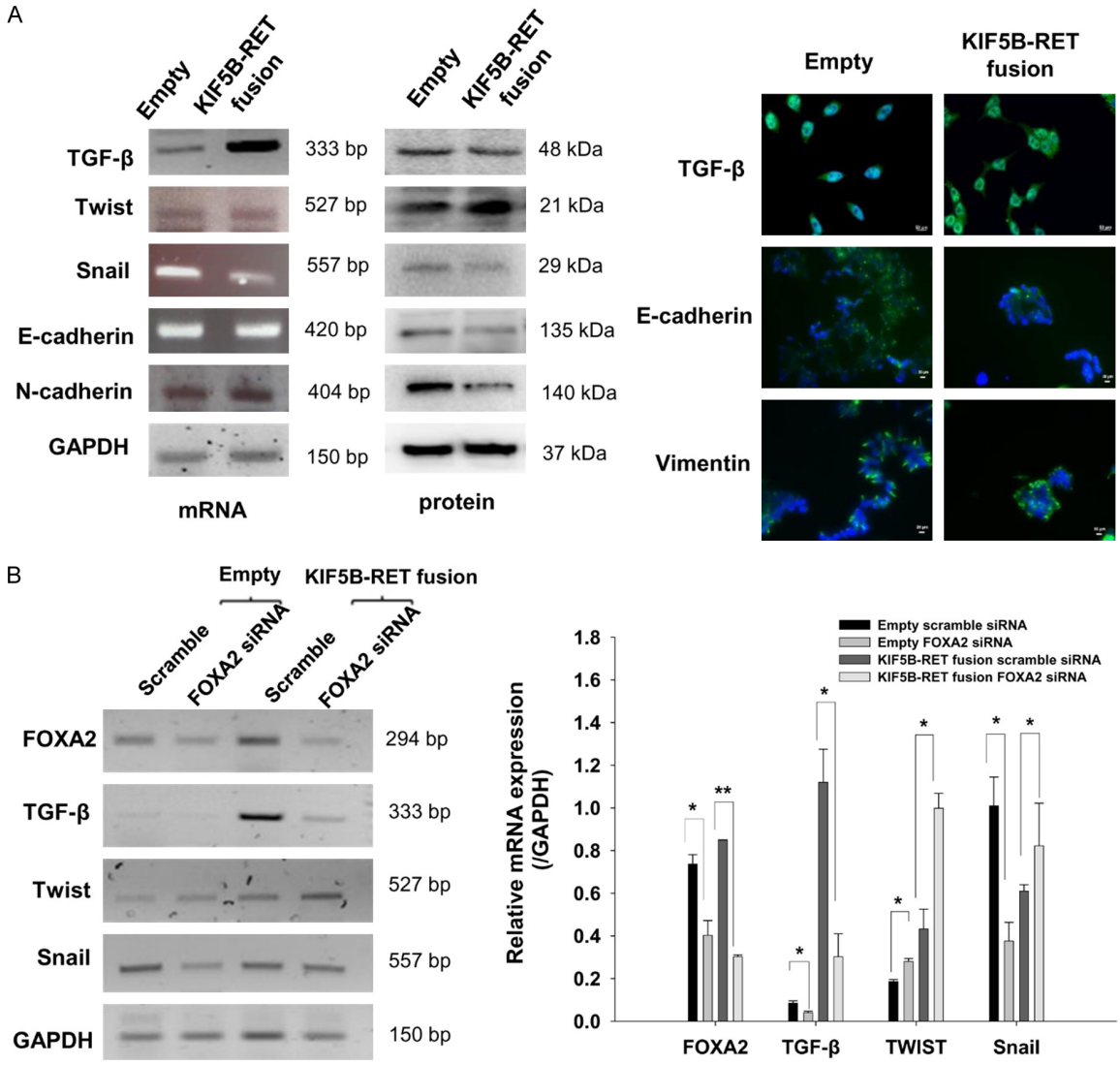

Figure 6. FOXA2 knockdown induces changes in the expression of EMT markers. A. EMT marker expression in KIF5B-RET gene fusion-containing cells was measured at the mRNA and protein levels (left) and immunofluorescence staining was performed for TGF-β1, E-cadherin, and Vimentin (right). B. Changes in the expression of TGF-β, Twist, and Snail mRNA following FOXA2 knockdown (left). Quantitative expression of mRNA (right). Data are presented as the mean ± SE. *denotes $P < 0.05$ and **denotes $P < 0.01$.

in vivo KIF5B-RET fusion models, we investigated the changes in cell morphology, proliferation, cell cycle, and downstream signaling molecules and identified putative transcription factors related to the EMT signaling pathway.

The phosphorylation of the cytoplasmic tyrosine residues of *RET* allows for the recruitment and binding of several adaptor molecules necessary for the subsequent activation of downstream signaling cascades, namely PI3K/AKT, RAS/RAF/MEK/ERK, JAK2/STAT3, and PKC pathways. When *RET* fusion occurs, it is sufficient for RET downstream signaling to drive even without ligand binding [27-31].

RAS-RAF-MEK-ERK signaling is required for both cyclin D expression and the assembly of the cyclin D-CDK4 complex in many cancer cell types. The activation of p-ERK is necessary for entry into the S phase and should be translocated from the cytoplasm to the nucleus [32]. David B. Solit et al. reported that treatment of B-RAF mutant cell lines with a specific MEK inhibitor caused a marked decline in cyclin D protein levels, followed by the loss of RB phosphorylation and profound G1 cell cycle arrest [33].

Our results indicated that the expression of p-ERK was increased in KIF5B-RET fusion cells,

while the expression of cyclin D1 and E2 was decreased, contradicting previous presentations [32, 33]. Thus, it is presumed that in the early stages of cell culture, the p-ERK protein is mainly located in the cytoplasm and not in the nucleus. However, as time passes, the activated p-ERK protein promotes the G1 phase by increasing the expression of the cyclin D1 protein as it is translocated into the nucleus. In contrast, in 3D spheroid cell culture and xenograft mice, KIF5B-RET fusion cells grew at a rapid rate when compared with 2D cell culture. In addition, we found that the expression of HIF-1α was very low in 2D cell culture (data not shown), whereas HIF-1α was expressed in large quantities in the tumor tissue from xenograft mice. It is well-known that HIF-1α induced by the hypoxic condition in various tumor tissues plays a key role in regulating cell proliferation. As cell culture was continued even after passing the 2D cell culture stage, cancer cell clumps became spheroids. At this time, HIF-1 induced in inner tumor cells under hypoxia may cause rapid tumor growth as a strong driver of cell proliferation.

We identified 1,172 genes with > 1.5-fold of differential RNA expression in KIF5-RET fusion cells using a cDNA microarray, while 359 putative target genes regulated by transcription factors exhibiting significantly differential expression in the TF PCR array, were determined. Six genes were identical in two gene sets. In addition, there were only six transcription factors showing consistently differential expression through the repeated TF PCR array experiments. Lastly, STAT5A and FOXA2, which have identified a common increase in expression in two candidate groups created by two different experimental tools, were selected. Thereafter, we confirmed that FOXA2 is highly expressed in both mRNA and protein levels in KIF5B-RET fusion cells.

STAT5A, *STAT5B*, and *STAT3* are closely related and are important regulators of cellular transformation as key components of the JAK/STAT signaling pathway [14, 34]. Also, they control cell proliferation and survival by regulating the expression of *CCND1*, *MYC*, *AKT1*, etc. [12]. Thus, the pharmacologic inhibition of oncogenic STAT3 and STAT5A signaling is being investigated in castration-resistant prostate cancer and hematopoietic malignancies [34]. The lower expression of *STAT5A* in patients with liver cancer and metastatic breast cancer is known to be associated with rapid tumor growth and poor clinical prognosis [35]. A previous study reported that cell proliferation was inhibited in STAT5A-overexpressed liver cancer cells with a significantly increased G0/G1 cell population and a decreased G2/M cell population, and cell migration was reduced [36].

Interestingly, in KIF5B-RET fusion cells with high expression of STAT5A mRNA and protein, we identified the change of cell morphology, significantly reduced cell proliferation with increased G0/G1 cell population by the remarkable inhibition of cyclin D1 and E2 and decreased migration capability. These findings suggest that *STAT5A* may play a major role in cellular transformation and cell proliferation during the early stage of cell culture. Additionally, we checked that the STAT5A protein was stained at a relatively higher level in *KIF5B-RET* fusion-positive xenograft mice and lung cancer patients harboring *RET* rearrangement.

FOXA2, a major transcription factor for bronchial epithelial cell differentiation, is a target gene for *CCAAT/enhancer binding protein α* (*C/EBPα*) transcription factor [18, 37-39]. The frequent downregulation of *FOXA2* through epigenetic silencing has been reported in lung cancer. Given the changes in *FOXA2* mRNA expression and the location of FOXA2 proteins observed in KIF5-RET fusion cells, after that cell proliferation progresses slowly during the early stage of cell culture, *FOXA2* mRNA induced by increased cell-to-cell contact is translated into abundant FOXA2 proteins in the nucleus, which is thought to regulate the transcription of target genes involved in cell proliferation and differentiation. In addition, we discovered that the FOXA2 protein was strongly stained, especially in the nuclei of tumor cells in advanced lung cancer patients carrying *RET* rearrangement and *KIF5B-RET* fusion-positive xenograft mice.

Halmos et al. suggested that *FOXA2* is a tumor suppressor gene on the basis of their observation that decreased cell growth, arrest of cell proliferation, and cell death occurred when FOXA2 expression was induced in lung cancer cells [18]. However, B. Wang et al. later reported that FOXA2 was highly expressed in colon cancer tissues and was mainly limited to the

nucleus and promoted cancer progressions such as cell proliferation, cell migration, and invasion [40], which is consistent with our results.

It is well-known that *TGF-β* is an important regulator of EMT and induces an increase in the migration ability of lung cancer cells. However, whether *FOXA2* is involved in *TGF-β1*-mediated EMT and cancer invasiveness remains still unclear. Previous studies reported that the high expression of FOXA2 correlates with the epithelial cell phenotype and suppresses TGF-β1-induced EMT and cell invasion by regulating the transcription of E-cadherin in human breast and lung cancer cells [41, 42].

We evaluated the expressions of EMT-related molecules, including *TGF-β, Snail, Twist, E-cadherin*, and *N-cadherin* in KIF5B-RET fusion cells. *TGF-β* mRNA was abundantly expressed and TGF-β proteins were mainly accumulated in the nucleus rather than in the cytosol. Twist expression was greatly increased at the protein level, whereas *Snail* expression was reduced to almost invisible levels. The expression of both E-cadherin and N-cadherin expression was reduced at the protein level.

When KIF5B-RET fusion cells were transiently transfected with synthetic siRNA against *FOXA2*, *TGF-β* mRNA expression was greatly reduced to almost invisible levels, whereas the expression of *Twist1* mRNA was significantly increased with a slight increase in *Snail* mRNA. Our results indicate that *FOXA2* regulates *TGF-β* expression at the transcription level and affects the expression of *Twist* and *Snail* mRNA. A previous study reported that *FOXA2* knockdown in lung cancer cells induced EMT markers and promoted cancer invasion by the increased expression of *Twist1* and *Snail*, which is consistent with our findings [42, 43]. Song et al. reported that the double knockdown of *FOXA1* and *FOXA2* in pancreatic cancer cells is essential for inducing EMT with a decline in E-cadherin expression [23]. In our study, neither *E-cadherin* nor *Snail* mRNA expression was significantly upregulated, indicating that transient FOXA2 inhibition could initiate the loss of epithelial traits; however, it was not sufficient to induce the mesenchymal phenotype.

Twist plays an important role in the complicated process of cancer metastasis, like angiogenesis, invadopodia, extravasation, chromosomal instability, and resistance against platinum compounds [44]. It is activated by a variety of intracellular signal cascades, including the Akt, STAT3, MAP kinase, Ras, and Wnt signaling pathways [45, 46]. Given the significant increase in p-BRAF, p-AKT, and p-ERK protein expression observed in KIF5B-RET fusion cells, noticeable increments in twisted protein levels are thought to be due to the continuous activation of multiple RET downstream signaling cascades, including PI3K/AKT, RAS/RAF/MEK/ERK, and JAK2/STAT3.

Snail not only induces EMT but is also associated with TGF-β signaling, the tumor grade, and nodal metastasis in metastatic cancer. It also induces cancer recurrence and drug resistance, which is related to a poor prognosis [47-49]. We observed that there were no changes in *Snail* expression as the cell density increased, suggesting that *TGF-β* induced by the KIF5B-RET gene fusion induced *Snail* expression, which may affect the expression of other EMT markers.

Our study has some limitations. First, because we experimented with HEK293T cells in which *KIF5B-RET* gene fusion was introduced, it was difficult to compare our results with other investigators' findings using cancer cell lines. Second, additional experiments on other molecules besides HIF1α are required to identify the rapid increase in cell proliferation in 3-dimensional culture and xenograft models. Third, the functions of *STAT5A* on cell proliferation, cell cycle, and migration should be elucidated.

In summary, in transformed HEK293T cells with the KIF5B-RET gene fusion, rapid cell proliferation and invasiveness are induced by the upregulation of STAT5A and FOXA2 through the continuous activation of RET downstream signal cascades, including ERK and AKT signaling pathways. The markedly increased *TGF-β1* mRNA found in KIF5B-RET fusion cells is regulated at the transcriptional level by *FOXA2*. Therefore, further studies on the association of FOXA and STAT5A with EMT in lung cancer cells carrying KIF5B-RET fusion are needed.

Acknowledgements

This work was supported by the National Research Foundation of Korea (NRF) grant

funded by the Korean government (MSIT; No. NRF-2017R1D1A1B04033954). The authors would like to thank Enago (www.enago.co.kr) for the English language review.

Written informed consent was obtained from all participants, and this study was approved by the Institutional Review Board of Seoul St. Mary's Hospital (approval No. KC15EISI0167).

Disclosure of conflict of interest

None.

Address correspondence to: Dr. Jinhyoung Kang, Department of Medical Oncology, Seoul St. Mary's Hospital, The Catholic University of Korea, 222 Banpo-daero Seocho-gu, Seoul, Republic of Korea. Tel: +82-2-2258-6043; Fax: +82-2-594-6043; E-mail: oncologykang@naver.com

References

[1] Ibáñez CF. Structure and physiology of the RET receptor tyrosine kinase. Cold Spring Harb Perspect Biol 2013; 5: a009134.

[2] Jhiang SM. The RET proto-oncogene in human cancers. Oncogene 2000; 19: 5590-5597.

[3] Lipson D, Capelletti M, Yelensky R, Otto G, Parker A, Jarosz M, Curran JA, Balasubramanian S, Bloom T, Brennan KW, Donahue A, Downing SR, Frampton GM, Garcia L, Juhn F, Mitchell KC, White E, White J, Zwirko Z, Peretz T, Nechushtan H, Soussan-Gutman L, Kim J, Sasaki H, Kim HR, Park SI, Ercan D, Sheehan CE, Ross JS, Cronin MT, Jänne PA and Stephens PJ. Identification of new ALK and RET gene fusions from colorectal and lung cancer biopsies. Nat Med 2012; 18: 382-384.

[4] Zhou L, Li J, Zhang X, Xu Z, Yan Y and Hu K. An integrative pan cancer analysis of RET aberrations and their potential clinical implications. Sci Rep 2022; 12: 13913.

[5] Cong XF, Yang L, Chen C and Liu Z. KIF5B-RET fusion gene and its correlation with clinicopathological and prognostic features in lung cancer: a meta-analysis. Onco Targets Ther 2019; 12: 4533-4542.

[6] Kim JO, Shin JY, Kim MY, Son KH, Jung CK, Kim TJ, Kim SY, Park JK, Sung SW, Bae SJ, Min HJ and Kang JH. Detection of RET (rearranged during transfection) variants and their downstream signal molecules in RET rearranged lung adenocarcinoma patients. Surg Oncol 2018; 27: 106-113.

[7] Sarfaty M, Moore A, Neiman V, Dudnik E, Ilouze M, Gottfried M, Katznelson R, Nechushtan H, Sorotsky HG, Paz K, Katz A, Saute M, Wolner M, Moskovitz M, Miller V, Elvin J, Lipson D, Ali S, Gutman LS, Dvir A, Gordon N and Peled N. RET fusion lung carcinoma: response to therapy and clinical features in a case series of 14 patients. Clin Lung Cancer 2017; 18: e223-e232.

[8] Drusbosky LM, Rodriguez E, Dawar R and Ikpeazu CV. Therapeutic strategies in RET gene rearranged non-small cell lung cancer. J Hematol Oncol 2021; 14: 50.

[9] Ju YS, Lee WC, Shin JY, Lee S, Bleazard T, Won JK, Kim YT, Kim JI, Kang JH and Seo JS. A transforming KIF5B and RET gene fusion in lung adenocarcinoma revealed from whole-genome and transcriptome sequencing. Genome Res 2012; 22: 436-445.

[10] Li F, Feng Y, Fang R, Fang Z, Xia J, Han X, Liu XY, Chen H, Liu H and Ji H. Identification of RET gene fusion by exon array analyses in "pan-negative" lung cancer from never smokers. Cell Res 2012; 22: 928-931.

[11] Kohno T, Ichikawa H, Totoki Y, Yasuda K, Hiramoto M, Nammo T, Sakamoto H, Tsuta K, Furuta K, Shimada Y, Iwakawa R, Ogiwara H, Oike T, Enari M, Schetter AJ, Okayama H, Haugen A, Skaug V, Chiku S, Yamanaka I, Arai Y, Watanabe S, Sekine I, Ogawa S, Harris CC, Tsuda H, Yoshida T, Yokota J and Shibata T. KIF5B-RET fusions in lung adenocarcinoma. Nat Med 2012; 18: 375-377.

[12] Igelmann S, Neubauer HA and Ferbeyre G. STAT3 and STAT5 activation in solid cancers. Cancers (Basel) 2019; 11: 1428.

[13] Wingelhofer B, Neubauer HA, Valent P, Han X, Constantinescu SN, Gunning PT, Müller M and Moriggl R. Implications of STAT3 and STAT5 signaling on gene regulation and chromatin remodeling in hematopoietic cancer. Leukemia 2018; 32: 1713-1726.

[14] Mohanty SK, Yagiz K, Pradhan D, Luthringer DJ, Amin MB, Alkan S and Cinar B. STAT3 and STAT5A are potential therapeutic targets in castration-resistant prostate cancer. Oncotarget 2017; 8: 85997-86010.

[15] Wan H, Dingle S, Xu Y, Besnard V, Kaestner KH, Ang SL, Wert S, Stahlman MT and Whitsett JA. Compensatory roles of Foxa1 and Foxa2 during lung morphogenesis. J Biol Chem 2005; 280: 13809-13816.

[16] Wan H, Xu Y, Ikegami M, Stahlman MT, Kaestner KH, Ang SL and Whitsett JA. Foxa2 is required for transition to air breathing at birth. Proc Natl Acad Sci U S A 2004; 101: 14449-14454.

[17] Ikeda K, Shaw-White JR, Wert SE and Whitsett JA. Hepatocyte nuclear factor 3 activates transcription of thyroid transcription factor 1 in respiratory epithelial cells. Mol Cell Biol 1996; 16: 3626-3636.

[18] Halmos B, Bassères DS, Monti S, D'Aló F, Dayaram T, Ferenczi K, Wouters BJ, Huettner CS, Golub TR and Tenen DG. A transcriptional profiling study of CCAAT/enhancer binding protein targets identifies hepatocyte nuclear factor 3β as a novel tumor suppressor in lung cancer. Cancer Res 2004; 64: 4137-4147.
[19] Kondratyeva LG, Sveshnikova AA, Grankina EV, Chernov IP, Kopantseva MR, Kopantzev EP and Sverdlov ED. Downregulation of expression of mater genes SOX9, FOXA2, and GATA4 in pancreatic cancer cells stimulated with TGFβ1 epithelial-mesenchymal transition. Dokl Biochem Biophys 2016; 469: 257-259.
[20] Perez-Balaguer A, Ortiz-Martínez F, García-Martínez A, Pomares-Navarro C, Lerma E and Peiró G. FOXA2 mRNA expression is associated with relapse in patients with triple-negative/basal-like breast carcinoma. Breast Cancer Res Treat 2015; 153: 465-474.
[21] Gao H, Yan Z, Sun H and Chen Y. FoXA2 promotes esophageal squamous cell carcinoma progression by ZEB2 activation. World J Surg Oncol 2021; 19: 286.
[22] Camolotto SA, Pattabiraman S, Mosbruger TL, Jones A, Belova VK, Orstad G, Streiff M, Salmond L, Stubben C, Kaestner KH and Snyder EL. FoxA1 and FoxA2 drive gastric differentiation and suppress squamous identity in NKX2-1-negative lung cancer. Elife 2018; 7: e38579.
[23] Song Y, Washington MK and Crawford HC. Loss of FOXA1/2 is essential for the epithelial-to-mesenchymal transition in pancreatic cancer. Cancer Res 2010; 70: 2115-2125.
[24] Huang C, Liu J, Xiong B, Yonemura Y and Yang X. Expression and prognosis analyses of forkhead box A (FOXA) family in human lung cancer. Gene 2019; 685: 202-210.
[25] Wang R, Hu H, Pan Y, Li Y, Ye T, Li C, Luo X, Wang L, Li H, Zhang Y, Li F, Lu Y, Lu Q, Xu J, Garfield D, Shen L, Ji H, Pao W, Sun Y and Chen H. RET fusions define a unique molecular and clinicopathologic subtype of non-small-cell lung cancer. J Clin Oncol 2012; 30: 4352-4359.
[26] Tsuta K, Kohno T, Yoshida A, Shimada Y, Asamura H, Furuta K and Kushima R. RET-rearranged non-small-cell lung carcinoma: a clinicopathological and molecular analysis. Br J Cancer 2014; 110: 1571-1578.
[27] Alberti L, Borrello MG, Ghizzoni S, Torriti F, Rizzetti MG and Pierotti MA. Grb2 binding to the different isoforms of Ret tyrosine kinase. Oncogene 1998; 17: 1079-1087.
[28] Schuringa JJ, Wojtachnio K, Hagens W, Vellenga E, Buys CH, Hofstra R and Kruijer W. MEN2A-RET-induced cellular transformation by activation of STAT3. Oncogene 2001; 20: 5350-5358.
[29] Asai N, Murakami H, Iwashita T and Takahashi M. A mutation at tyrosine 1062 in MEN2A-Ret and MEN2B-Ret impairs their transforming activity and association with shc adaptor proteins. J Biol Chem 1996; 271: 17644-17649.
[30] Liu X, Vega QC, Decker RA, Pandey A, Worby CA and Dixon JE. Oncogenic RET receptors display different autophosphorylation sites and substrate binding specificities. J Biol Chem 1996; 271: 5309-5312.
[31] Perrinjaquet M, Vilar M and Ibáñez CF. Protein-tyrosine phosphatase SHP2 contributes to GDNF neurotrophic activity through direct binding to phospho-Tyr687 in the RET receptor tyrosine kinase. J Biol Chem 2010; 285: 31867-31875.
[32] Torii S, Yamamoto T, Tsuchiya Y and Nishida E. ERK MAP kinase in G1 cell cycle progression and cancer. Cancer Sci 2006; 97: 697-702.
[33] Solit DB, Garraway LA, Pratilas CA, Sawai A, Getz G, Basso A, Ye Q, Lobo JM, She Y, Osman I, Golub TR, Sebolt-Leopold J, Sellers WR and Rosen N. BRAF mutation predicts sensitivity to MEK inhibition. Nature 2006; 439: 358-362.
[34] Brachet-Botineau M, Polomski M, Neubauer HA, Juen L, Hédou D, Viaud-Massuard MC, Prié G and Gouilleux F. Pharmacological inhibition of oncogenic STAT3 and STAT5 signaling in hematopoietic cancers. Cancers (Basel) 2020; 12: 240.
[35] Peck AR, Witkiewicz AK, Liu C, Klimowicz AC, Stringer GA, Pequignot E, Freydin B, Yang N, Ertel A, Tran TH, Girondo MA, Rosenberg AL, Hooke JA, Kovatich AJ, Shriver CD, Rimm DL, Magliocco AM, Hyslop T and Rui H. Low levels of Stat5a protein in breast cancer are associated with tumor progression and unfavorable clinical outcomes. Breast Cancer Res 2012; 14: R130.
[36] Jiang Y, Tao Y, Zhang X, Wei X, Li M, He X, Zhou B, Guo W, Yin H and Cheng S. Loss of STAT5A promotes glucose metabolism and tumor growth through miRNA-23a-AKT signaling in hepatocellular carcinoma. Mol Oncol 2021; 15: 710-724.
[37] An JH, Jang SM, Kim JW, Kim CH, Song PI and Choi KH. The expression of p21 is upregulated by forkhead box A1/2 in p53-null H1299 cells. FEBS Lett 2014; 588: 4065-4070.
[38] Basseres DS, D'Alò F, Yeap BY, Löwenberg EC, Gonzalez DA, Yasuda H, Dayaram T, Kocher ON, Godleski JJ, Richards WG, Meyerson M, Kobayashi S, Tenen DG, Halmos B and Costa DB. Frequent downregulation of the transcription factor Foxa2 in lung cancer through epigenetic silencing. Lung Cancer 2012; 77: 31-37.
[39] Jang SM, An JH, Kim CH, Kim JW and Choi KH. Transcription factor FOXA2-centered transcriptional regulation network in non-small cell lung

cancer. Biochem Biophys Res Commun 2015; 463: 961-967.
[40] Wang B, Liu G, Ding L, Zhao J and Lu Y. FOXA2 promotes the proliferation, migration and invasion, and epithelial mesenchymal transition in colon cancer. Exp Ther Med 2018; 16: 133-140.
[41] Zhang Z, Yang C, Gao W, Chen T, Qian T, Hu J and Tan Y. FOXA2 attenuates the epithelial to mesenchymal transition by regulating the transcription of E-cadherin and ZEB2 in human breast cancer. Cancer Lett 2015; 361: 240-250.
[42] Tang Y, Shu G, Yuan X, Jing N and Song J. FOXA2 functions as a suppressor of tumor metastasis by inhibition of epithelial-to-mesenchymal transition in human lung cancers. Cell Res 2011; 21: 316-326.
[43] Bow YD, Wang YY, Chen YK, Su CW, Hsu CW, Xiao LY, Yuan SS and Li RN. Silencing of FOXA2 decreases E-cadherin expression and is associated with lymph node metastasis in oral cancer. Oral Dis 2020; 26: 756-765.
[44] Khan MA, Chen HC, Zhang D and Fu J. Twist: a molecular target in cancer therapeutics. Tumour Biol 2013; 34: 2497-2506.
[45] Roberts CM, Tran MA, Pitruzzello MC, Wen W, Loeza J, Dellinger TH, Mor G and Glackin CA. TWIST1 drives cisplatin resistance and cell survival in an ovarian cancer model, via upregulation of GAS6, L1CAM, and Akt signalling. Sci Rep 2016; 6: 37652.
[46] Zhuo WL, Wang Y, Zhuo XL, Zhang YS and Chen ZT. Short interfering RNA directed against TWIST, a novel zinc finger transcription factor, increases A549 cell sensitivity to cisplatin via MAPK/mitochondrial pathway. Biochem Biophys Res Commun 2008; 369: 1098-1102.
[47] Shin NR, Jeong EH, Choi CI, Moon HJ, Kwon CH, Chu IS, Kim GH, Jeon TY, Kim DH, Lee JH and Park DY. Overexpression of Snail is associated with lymph node metastasis and poor prognosis in patients with gastric cancer. BMC Cancer 2012; 12: 521.
[48] Naber HP, Drabsch Y, Snaar-Jagalska BE, ten Dijke P and van Laar T. Snail and Slug, key regulators of TGF-β-induced EMT, are sufficient for the induction of single-cell invasion. Biochem Biophys Res Commun 2013; 435: 58-63.
[49] Jin H, Yu Y, Zhang T, Zhou X, Zhou J, Jia L, Wu Y, Zhou BP and Feng Y. Snail is critical for tumor growth and metastasis of ovarian carcinoma. Int J Cancer 2010; 126: 2102-2111.

Table S1. The DNA sequence of individual set of primers

Primer	Stand	Sequence (5' → 3')
TGFβ1	Forward	GCCCTGGAGACCAACTATTGC
	Reverse	GCACTTGCAGGAGCGCA
twist1	Forward	TCTCGGTCTGGAGGATGGAG
	Reverse	GTTATCCAGCTCCAGAGTCT
Snail	Forward	CAGACCCACTCAGATGTCAA
	Reverse	CATAGTTAGTCACACCTCGT
N-cadherin	Forward	GATGTTGAGGTACAGAATCGT
	Reverse	GGTCGGTCTGGATGGCGA
E-cadherin	Forward	TGAGAGTTGCACCGGTGCAC
	Reverse	TCTCTCACGCTGTGTCATCC
FOXA2	Forward	CCACCACCAACCCCACAAAATG
	Reverse	TGCAACACCGTCTCCCCAAAGT
GAPDH	Forward	TGGACTCCACGACGTACTCAG
	Reverse	ACATGTTCCAATATGATTCCA

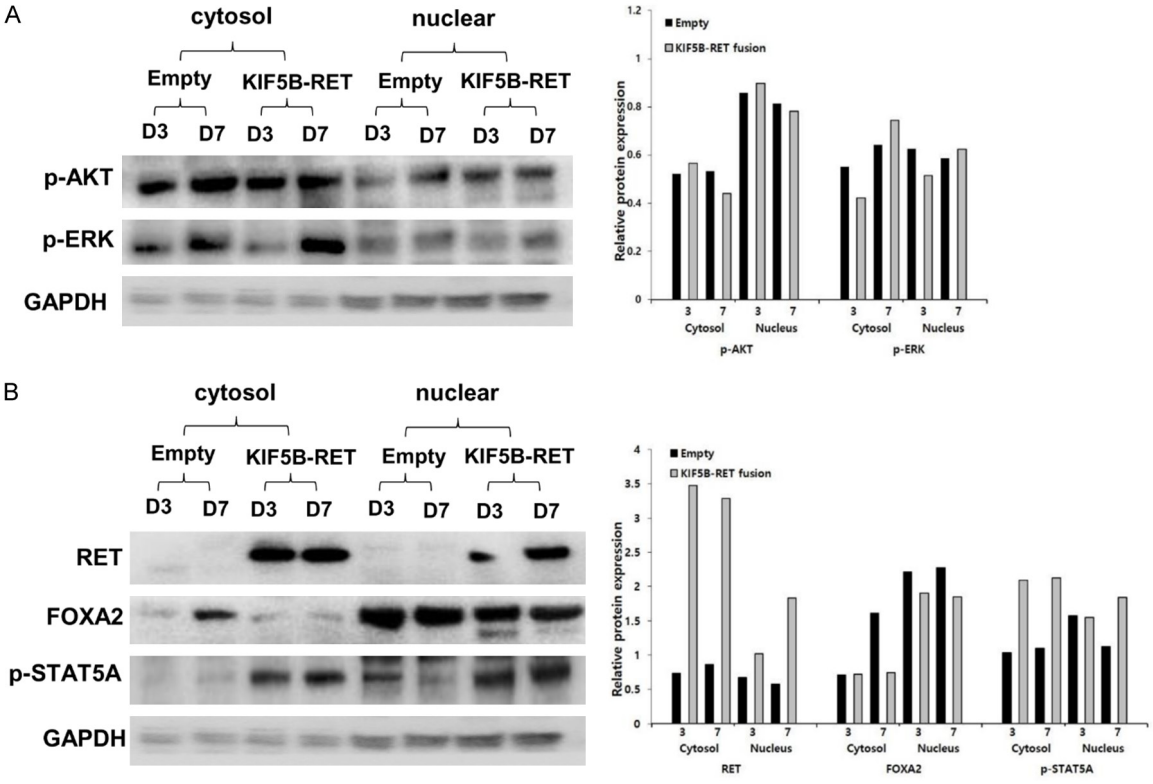

Figure S1. Identification of RET downstream molecules and FOXA2, STAT5A expression harboring KIF5B-RET fusion gene in cytoplasm and nucleus. (A) RET downstream signaling molecules and (B) FOXA2, STAT5A and RET were identified in the cytoplasm and in the nucleus. Quantitative expression of protein (right). The data are presented as the mean ± SE.

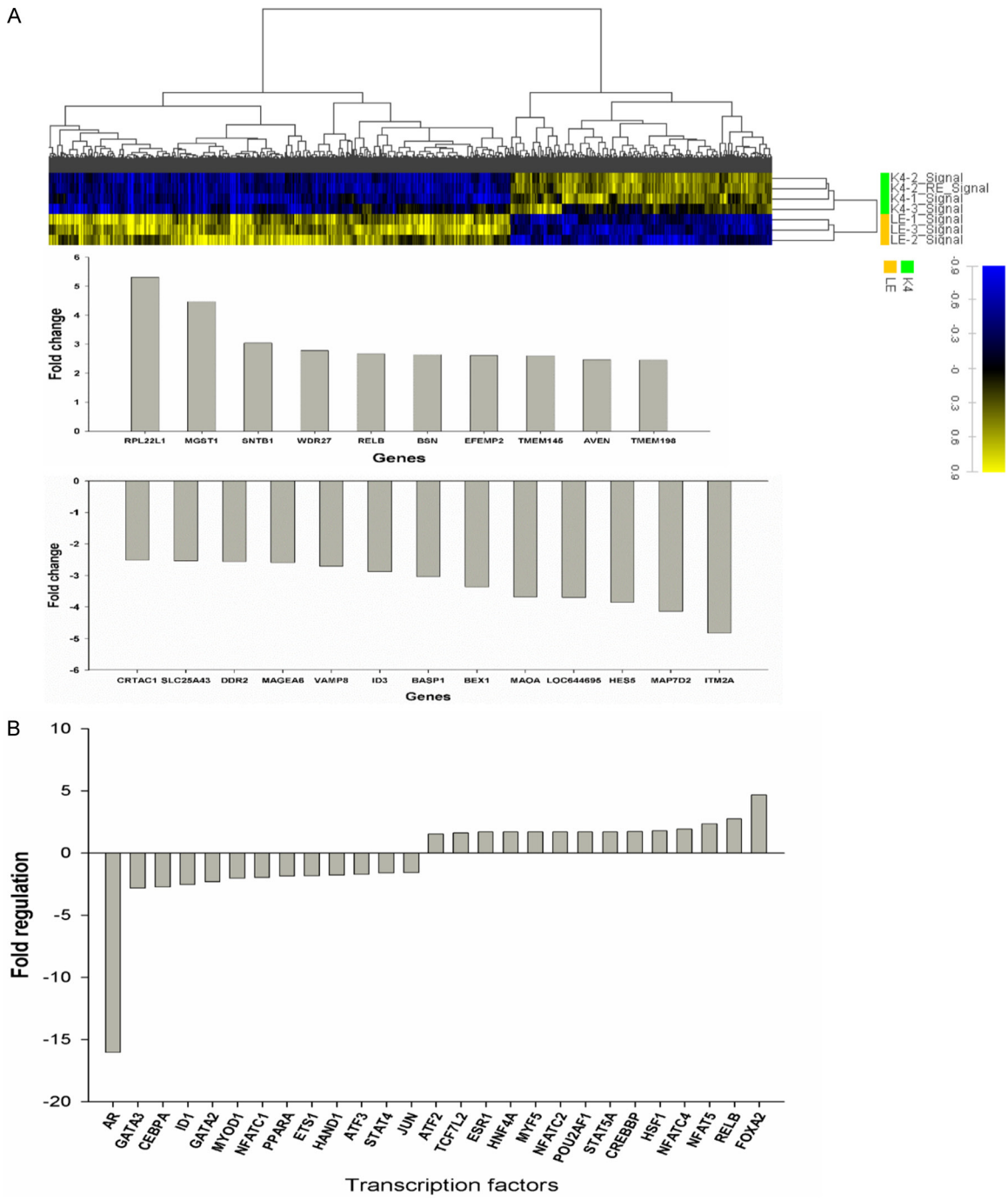

Figure S2. Transcription factors up-regulated in KIF5B-RET fusion gene. (A) The cDNA microarray and (B) transcription factor PCR array, identified the expression of genes and transcription factors for the purpose of identifying down-stream signaling molecules influenced by the KIF5B-RET fusion-gene.

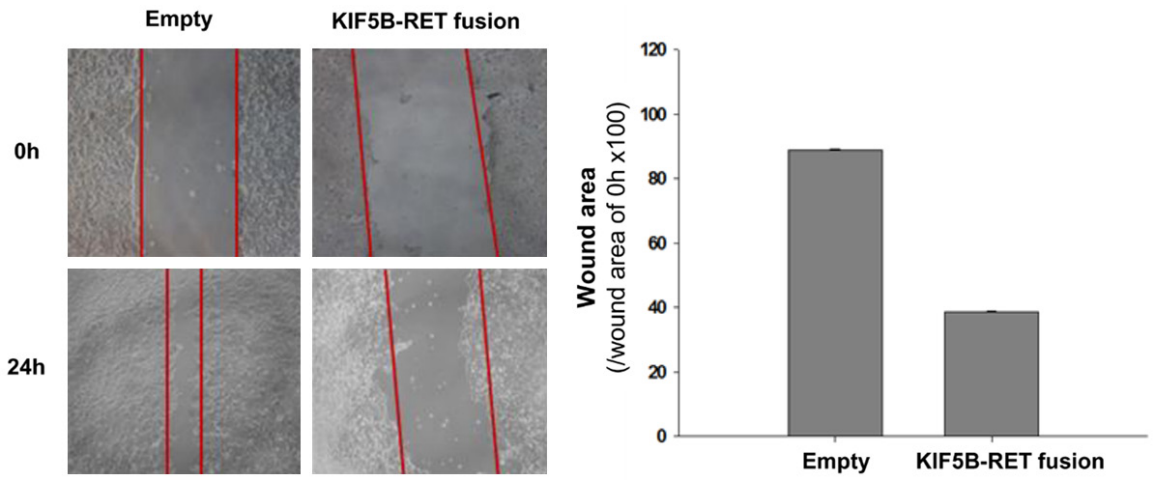

Figure S3. Decreased cell proliferation and migration ability in the KIF5B-RET fusion gene. Representative images of the scratched areas and the recovery of wounded areas (marked by red lines) in confluent monolayers of empty vector and KIF5B-RET fusion cells after 24 h. Values of the percent wound area (right). The data are presented as the mean ± SE.

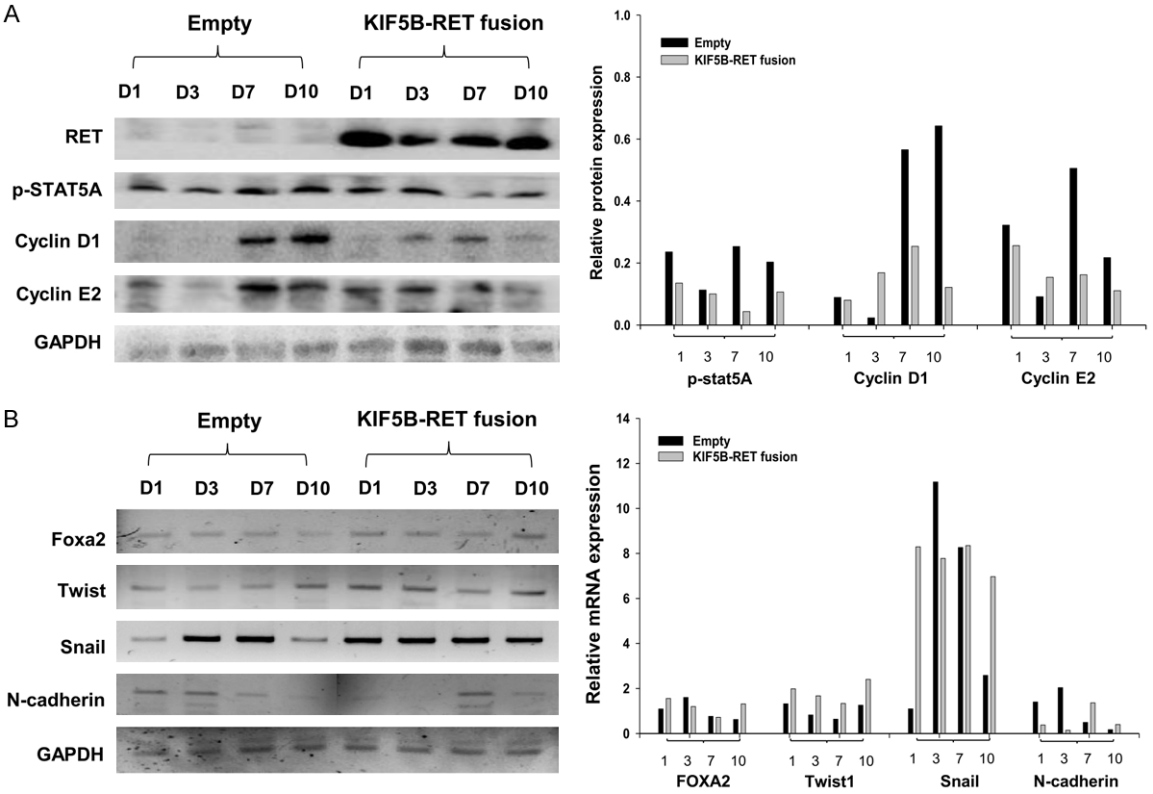

Figure S4. Identification of cell cycle and EMT marker expression in KIF5B-RET fusion gene. A. The level of cell cycle-related molecules including RET, p-STAT5A by western blot analysis over time. B. EMT markers were identified by RT-PCR over time. Quantitative expression of protein (right). The data are presented as the mean ± SE.